LLNL-JRNL-692260

LAWRENCE LIVERMORE NATIONAL LABORATORY

Impact of Decadal Cloud Variations on the Earth's Energy Budget

C. Zhou, M. D. Zelinka, S. A. Klein

May 17, 2016

Nature-geoscience

Impact of decadal cloud variations on the Earth's energy budget

Chen Zhou*, Mark D. Zelinka, and Stephen A. Klein

Lawrence Livermore National Laboratory, Livermore, CA, USA

*zhou8@llnl.gov

Feedbacks of clouds on climate change strongly influence the magnitude of global warming[1-3]. Cloud feedbacks, in turn, depend on the spatial patterns of surface warming[4-9], which vary on decadal timescales. Therefore, the magnitude of the decadal cloud feedback could deviate from the long-term cloud feedback[4]. Here we present climate model simulations to show that the global mean cloud feedback in response to decadal temperature fluctuations varies dramatically due to time variations in the spatial pattern of sea surface temperature (SST). We find that cloud anomalies associated with these patterns significantly modify the Earth's energy budget. Specifically, the decadal cloud feedback between the 1980s and 2000s is substantially more negative than the long-term cloud feedback. This is a result of cooling in tropical regions where air descends, relative to warming in tropical ascent regions, which strengthens low-level atmospheric stability. Under these conditions, low-level cloud cover and its reflection of solar radiation increase, despite an increase in global mean surface temperature. These results suggest that SST pattern-induced low cloud anomalies could have contributed to the period of reduced

warming between 1998 and 2013, and offer a physical explanation of why climate sensitivities estimated from recently observed trends are probably biased low[4].

Clouds play a significant role in the earth's climate system by reflecting incoming solar radiation and reducing outgoing thermal radiation. As the earth's surface warms, the net radiative effect of clouds also changes, contributing a feedback to the climate system.

Recent studies suggest that the magnitude of climate feedbacks depend on surface warming patterns[4-9]. Therefore we expect that the magnitude of decadal cloud feedback deviates from the long-term cloud feedback due to decadal variations in the spatial pattern of SST anomalies[4], and may play a non-negligible role in decadal climate variability[10]. In this study, we perform idealized experiments to gain insight into the causes of decadal cloud variations over the last century. We then test the robustness of our experimental results by examining cloud trends during the satellite era in Coupled Model Intercomparison Project Phase 5 (CMIP5)[11] - Atmospheric Model Intercomparison Project (AMIP) simulations, CMIP5-historical simulations, and observations.

Our experiments employ the Community Earth System model V1.2.1- Community Atmospheric Model 5.3 (CESM1.2.1-CAM5.3)[12] with a resolution of 1.9° longitude by 2.5° latitude. The control experiments ("AMIP-like", two runs with different initial conditions) use prescribed historical SST and climate forcings (aerosols, greenhouse gases, and solar radiation). To isolate the SST-driven component of cloud changes, we run two idealized "AMIPFF" experiments with historical SST but climate forcings fixed at pre-industrial and present day levels, respectively. To investigate the effect of spatial patterns of SST anomalies on clouds, two patterned SST experiments are carried out ("PSST"). The PSST experiments are identical to the AMIPFF experiments except that spatially uniform SST anomalies are subtracted from the historical SST at each time step to keep the global surface temperature roughly constant (see Methods). Historical sea ice is prescribed in all simulations. Confidence in CAM's simulation comes from its consistency with observations for the sensitivities of low cloud cover (LCC) to SST and estimated inversion strength (EIS)[13] and the recent evolution of cloud controlling factors and cloud-induced radiation anomalies (Supplementary Figures 1-3).

Our analysis begins with the decadal net feedback (climate feedback parameter), which is calculated as the regression slope of annual global TOA net flux anomalies against annual global surface temperature anomalies in AMIPFF simulations over 30-year windows. Figure 1(a) indicates that the 30-year feedback parameter varies dramatically and is significantly more negative than the long-term net feedback (see Methods) after 1980. This is consistent with HadGEM2A/HadCM3A simulations carried out by Gregory and Andrews[4] and with experiments we have conducted with CAM4 (Supplementary Figure 4), indicating that the decadal variations of net feedback are robust.

The variation of decadal net feedback is primarily induced by clouds (Fig. 1b, Supplementary Figure 5). Decadal cloud-induced radiation anomalies (ΔR_{cloud}, see Methods) vary dramatically throughout the AMIPFF simulations while the global surface temperature increases relatively steadily (Fig. 2a), resulting in variations of decadal cloud feedback (Fig. 1b) and the corresponding net feedback. To understand the causes of decadal R_{cloud} variations, we decompose the cloud induced radiation anomalies using the following equation

$$\Delta R_{cloud} = \lambda_c \Delta T_s + \Delta R_{PSST} + \Delta R_{cf} + \varepsilon\,, \tag{1}$$

where λ_c is the magnitude of cloud feedback under uniform SST warming (see Methods), T_s is global surface skin temperature, ΔR_{PSST} is the cloud-induced radiation anomaly in response to changes in SST pattern in absence of global mean temperature changes (= ΔR_{cloud} from PSST simulation), ΔR_{cf} is the rapid cloud radiative adjustment in response to changes in climate forcings (zero in our fixed forcing experiments), and ε is the error term. ΔR_{cloud} in the AMIPFF simulation is well correlated (r=0.93) with the sum of $\lambda_c \Delta T_s$ and ΔR_{PSST} terms (Fig. 2a). These results suggest that cloud feedback can be linearly decomposed into a fixed feedback under uniform warming, plus a SST pattern-induced component.

Figure 2(b) shows the decadal anomalies in global low cloud cover (LCC), which are primarily contributed from ΔLCC over the tropical oceans (Fig. 2c). The tropical marine ΔLCC in AMIPFF simulations is well correlated with and contributes significantly to variability in the global ΔR_{cloud} (r=-0.77). These low clouds strongly cool the Earth's climate system and play an important role in determining the magnitude of cloud feedback[14,15,16,9].

We explain tropical marine ΔLCC with cloud controlling factors. An increase in EIS or decrease of SST would contribute positively to LCC[16,17,18,9], so tropical ΔLCC can be explained by the linear combination of tropical mean SST and EIS anomalies (Fig. 2c, r=0.76), with EIS anomalies explaining more decadal variance in LCC. Furthermore, changes in EIS are well explained (r=0.94) by a linear combination of the tropical mean SST[19] and the difference between SST in tropical strong ascent regions and the tropical mean SST (ΔT(up,trp), see Methods), with the latter explaining more decadal variance in EIS (Fig. 2d). Physically, EIS increases with this SST difference because free-tropospheric temperatures throughout the tropics are controlled by the moist adiabat set by the SST in tropical ascent regions[20], whereas SSTs in tropical descent regions only affect the temperature of boundary layer locally. As a result, LCC variations over the 20th century are primarily induced by the SST pattern instead of changes in tropical mean SST (Supplementary Text 1 and Supplementary Figure 6).

The above mechanism explains the abnormal decadal net feedback during the satellite era (1979-present), when surface warming is most pronounced over tropical ascent regions where deep convection occurs, with cooling over tropical descent regions, particularly in the Eastern Pacific where low clouds are common (Supplementary Figure 7). The pronounced warming in the tropical ascent regions causes the tropical troposphere to warm, and in the absence of equivalent warming in descent regions, causes the tropical EIS to increase significantly (Fig. 2d), contributing positively to the LCC trend. Meanwhile, the SST-induced LCC reduction over the broader tropical oceans is not strong enough to compensate the EIS induced LCC increase (Fig. 2c). Altogether, the positive tropical mean LCC trend results in a negative R_{cloud} trend (Fig. 2a), and hence a negative decadal cloud feedback during this period (Fig. 1b) because the negative R_{cloud} trend happens concurrently with a positive global mean surface temperature trend. SST, EIS, LCC, and R_{cloud} trends also exhibit a clear spatial correspondence, confirming the physical linkages among them (Supplementary Figure 8). As a result, the recent decadal feedback parameter is significantly more negative than the values under uniform or patterned long-term warming (Fig. 1a)[4].

To further demonstrate the importance of the SST pattern in driving LCC trends, we compare 1980-2005 LCC trends in AMIP with those in CMIP5-historical simulations (Supplementary Table 1). This comparison is valid because historical climate forcings are identically prescribed in both AMIP and CMIP5-historical simulations, meaning that differences are primarily the result of differing patterns of SST change between AMIP and CMIP5-historical simulations. In AMIP simulations, where the SST is the same as observations by design, there is significant LCC increase in the Eastern Pacific Ocean, Southern Indian Ocean, and Southern Atlantic Ocean (Fig. 3a, c), qualitatively consistent with artifact-corrected satellite observations[21,22] (Fig. 3e, Supplementary Figure 9). In contrast, SST warming is distributed more uniformly in CMIP5-historical (Fig. 3b, Supplementary Figure 10), and the model ensemble mean LCC trend is negative over much of the tropical regions (Fig. 3d). Averaging tropically or globally (Fig. 3f), the model ensemble mean LCC trend is positive in AMIP simulations, consistent with our CAM5.3 simulations, and negative in CMIP5-historical simulations, consistent with LCC changes under uniform and patterned long-term global warming (Supplementary Figure 11). These differences hold for individual models as well: Compared to historical simulations, the $\Delta T(up,trp)$ trend is systematically larger and the SST trend in descent regions is systematically smaller in AMIP simulations (Supplementary Figure 12), leading to systematically more positive EIS and LCC trends in AMIP than in historical simulations (Fig. 3f). Examination of climate model control simulations suggests that these systematic differences may not be explained purely by lack of synchronization between internally-generated trends in coupled historical simulations and those occurring in nature (Supplementary Text 2 and Supplementary Figure 13). If so, the 1980-2005 SST trend pattern is likely to be partly forced, with a potentially important role for aerosols[23,24]. On the other hand, if models collectively underestimate internal variability on decadal timescale, the possibility remains that the pattern was an unusual natural fluctuation that coupled models do not simulate.

The average SST pattern-induced component of ΔR_{cloud} is -0.35 W/m^2 during the 2000s (Fig. 2a), which is comparable to current TOA net flux anomaly (~0.6 W/m^2)[25]. To the extent that the global warming rate is affected by the TOA net flux imbalance[26], SST pattern-induced negative R_{cloud} anomalies -- together with oceanic heat storage at depth[23] and aerosol forcing[27,28] -- are likely to have contributed to the global warming hiatus in the 2000s.

In conclusion, SST pattern-induced cloud anomalies have an important impact on the Earth's energy budget. Until the signal of greenhouse gas induced warming dominates over the noise of internal variability, the SST pattern-induced cloud radiation anomalies will be at least as large as those that are due to global surface warming. Indeed, SST pattern-induced enhancements in cloud cooling have dominated over the past several decades in CAM5.3 despite it having a positive cloud feedback under long-term warming. The SST trend pattern over the last three decades exhibits much greater warming in tropical ascent regions relative to the broader tropics, in contrast to the more uniform warming that characterizes observed long-term (1871-2005) SST trends, nearly all historical simulations between 1980 and 2005, and future projections of CO_2-induced climate change (Supplementary Figure 7 and 10). Therefore, both the cloud feedback and net feedback computed from recent trends are much more negative than in response to long-term warming, indicating that climate sensitivity estimated from recent climate changes is likely to be underestimated if SST pattern-induced cloud anomalies are not accounted for.

References

1. Dufresne, J.-L. & Bony, S. An assessment of the primary sources of spread of global warming estimates from coupled atmosphere-ocean models. *Journal of Climate* **21**, 5135-5144 (2008).

2. Webb, M. J. *et al.* On the contribution of local feedback mechanisms to the range of climate sensitivity in two GCM ensembles. *Clim. Dyn.* **27**, 17–38 (2006).
3. Caldwell, P. M., Zelinka, M. D., Taylor, K. E. & Marvel, K. Quantifying the Sources of Intermodel Spread in Equilibrium Climate Sensitivity. *Journal of Climate* **29**, 513-524 (2016).
4. Gregory J. M. & Andrews, T. Variation in climate sensitivity and feedback parameters during the historical period. *Geophys. Res. Lett.* 43, 3911-3920 (2016).
5. Xie, S.-P., Kosaka, Y. & Okumura, Y. M. Distinct energy budgets for anthropogenic and natural changes during global warming hiatus. *Nature Geoscience* **9**, 29-33 (2016).
6. Armour, K. C., Bitz, C. M. & Roe, G. H. Time-varying climate sensitivity from regional feedbacks. *J. Climate* **26**, 4518-4534 (2013).
7. Andrews, T. Using an AGCM to Diagnose Historical Effective Radiative Forcing and Mechanisms of Recent Decadal Climate Change. *Journal of Climate* **27**, 1193-1209 (2014).
8. Andrews, T., Gregory, J. M. & Webb, M. J. The Dependence of Radiative Forcing and Feedback on Evolving Patterns of Surface Temperature Change in Climate Models. *Journal of Climate* **28**, 1630-1648 (2015).
9. Zhou, C., Zelinka, M. D., Dessler, A. E. & Klein, S. A. The relationship between interannual and long-term cloud feedbacks. *Geophys. Res. Lett.* **42**, 10463–10469 (2015).
10. Brown, P. T., Li, W., Li, L., & Ming, Y. Top-of-atmosphere radiative contribution to unforced decadal global temperature variability in climate models. *Geophys. Res. Lett.* **41**, 5175–5183 (2014).

11. Taylor K. E., Stouffer, R. J. & G. A. Meehl, G. A. An overview of CMIP5 and the experiment design. *Bull. Am. Meteorol. Soc.* **93**, 485–498 (2012).
12. http://www2.cesm.ucar.edu/
13. Wood, R., Bretherton C. S. On the relationship between stratiform low cloud cover and lower-tropospheric stability. *J. Clim.* **19**, 6425–6432 (2006).
14. Bony, S., & Dufresne, J. L. Marine boundary layer clouds at the heart of tropical cloud feedback uncertainties in climate models. *Geophys. Res. Lett.* **32**, L20806 (2005).
15. Soden, B. J. & Vecchi, G. A. The vertical distribution of cloud feedback in coupled ocean-atmosphere models. *Geophys. Res. Lett.* **38**, L12704 (2011).
16. Sherwood, S. C., Bony, S. & Dufresne, J.-L. Spread in model climate sensitivity traced to atmospheric convective mixing. *Nature* **505**, 37-42 (2014).
17. Qu, X., Hall, A., Klein, S. A. & DeAngelis, A. M. Positive tropical marine low-cloud cover feedback inferred from cloud-controlling factors. *Geophys. Res. Lett.* **42**, 7767-7775 (2015).
18. Bretherton, C. S. & Blossey, P. N. Low cloud reduction in a greenhouse-warmed climate: Results from Lagrangian LES of a subtropical marine cloudiness transition. *J. Adv. Model. Earth Syst.* 6, 91–114 (2014).
19. Qu, X., Hall, A., Klein, S. A. & Caldwell P. M., The strength of the tropical inversion and its response to climate change in 18 CMIP5 models. *Clim Dyn* **45**, 375-396 (2015).
20. Sobel, A. H., Nilsson, J. & Polvani, L. M., The Weak Temperature Gradient Approximation and Balanced Tropical Moisture Waves. *Journal of Atmospheric Sciences* **58**, 3650-3665 (2001).

21. Seethala, C., Norris, J. R., & Myers, T. A. How Has Subtropical Stratocumulus and Associated Meteorology Changed since the 1980s? *J. Climate* **28**, 8396-8410 (2015).

22. Norris, J. R. & Evan, A. T. Empirical Removal of Artifacts from the ISCCP and PATMOS-x Satellite Cloud Records. *Journal of Atmospheric and Oceanic Technology* **32**, 691-702 (2015).

23. Watanabe, M. *et al.* Contribution of natural decadal variability to global warming acceleration and hiatus. *Nature Climate Change* **4**, 893-897 (2014).

24. Takahashi C. & Watanabe M. Pacific trade winds accelerated by aerosol forcing over the past two decades. Nature Climate Change 6, 768-772 (2016).

25. Stephens, G. L. et al. An update on Earth's energy balance in light of the latest global observations. *Nature Geoscience* **5**, 691-696 (2012).

26. Smith, D. M., Allan, R. P., Coward, A. C., Eade, R., Hyder, P., Liu, C., Loeb, N. G., Palmer, M. D., Roberts, C. D. and Scaife, A. A. (2015), Earth's energy imbalance since 1960 in observations and CMIP5 models. Geophys. Res. Lett., 42: 1205-1213. doi: 10.1002/2014GL062669.

27. Santer, B. D. *et al.* Volcanic contribution to decadal changes in tropospheric temperature. *Nature Geoscience* **7**, 185-189 (2014).

28. Estrada, F., Perron, P. & Martinez-Lopez, B. Statistically derived contributions of diverse human influences to twentieth-century temperature changes. *Nature Geoscience* **6**, 1050-1055 (2013).

Acknowledgements:

The authors thank Dr. J. Norris for providing the corrected ISCCP and PATMOS-x data, and thank Drs. J. Gregory, A. Dessler, A. Hall, H. Su, X. Qu, C. Terai, and A. DeAngelis for valuable discussions. This work was supported by the Regional and Global Climate Modeling Program of the Office of Science at the U. S. Department of Energy (DOE) under the project "Identifying Robust Cloud Feedbacks in Observations and Models" and was performed under the auspices of DOE by Lawrence Livermore National Laboratory under Contract DE-AC52-07NA27344. IM Release #LLNL-JRNL-692260.

Author contributions

C. Z. performed the analysis. C. Z. and M. D. Z. designed the experiments. S. A. K. proposed the cloud analyses. The paper was discussed and written by all authors.

Competing financial interests

The authors declare no competing financial interests.

Figure Captions

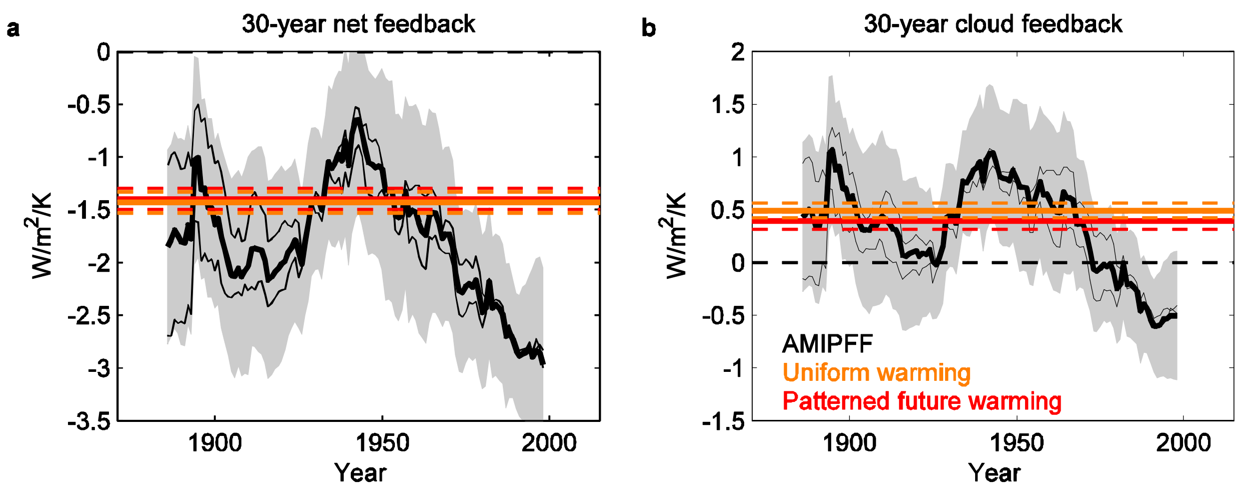

Figure 1. Evolution of decadal net and cloud feedbacks from CAM5.3 simulations. (a) 30-year net feedback estimates from AMIPFF simulations, plotted at the mid-point of each 30-year period. Thin black lines are calculated from individual runs, and thick black lines are calculated from ensemble mean values. Horizontal solid lines denote the long-term cloud feedbacks computed from uniform (orange) and patterned (red) future warming experiments (see Methods). Dashed red/orange lines and grey shading denote 2σ uncertainty intervals. (b) Same as (a), but for the cloud feedback.

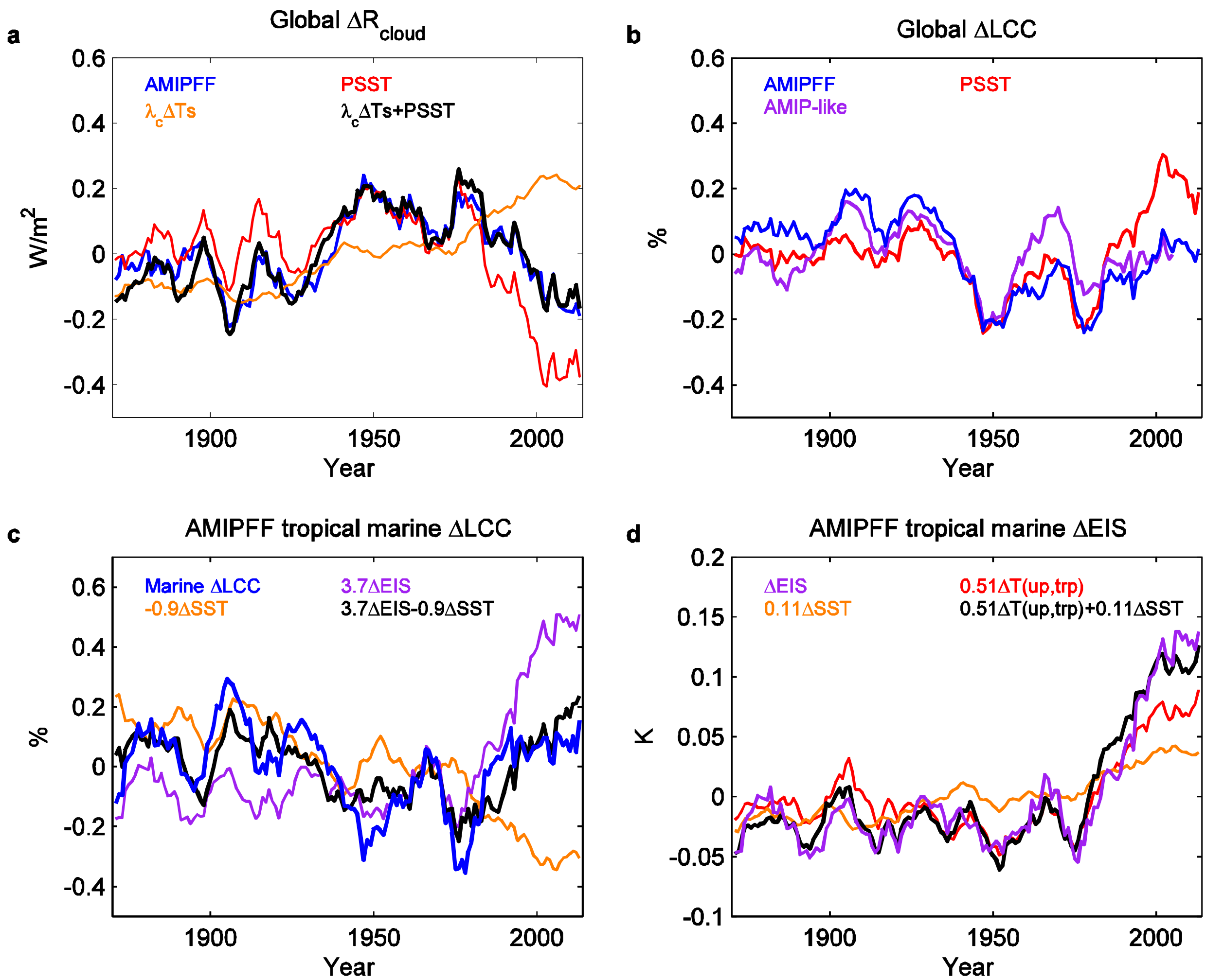

Figure 2. Evolution of selected 9-year moving averaged quantities from CAM5.3 simulations. (a) Global cloud-induced radiation anomaly in AMIPFF simulations (blue), its components due to anomalies in SST pattern (red) and global mean surface temperature (orange), and their sum (black). (b) Global low cloud cover anomalies (ΔLCC) in all simulations. (c) Tropical marine ΔLCC in AMIPFF simulations (blue), its components due to estimated inversion strength anomalies (ΔEIS) (purple), ΔSST (orange), and their sum (black). (d) Tropical marine ΔEIS in AMIPFF simulations (purple), its components due to ΔT(up,trp) (red, see Methods), ΔSST (orange), and their sum (black).

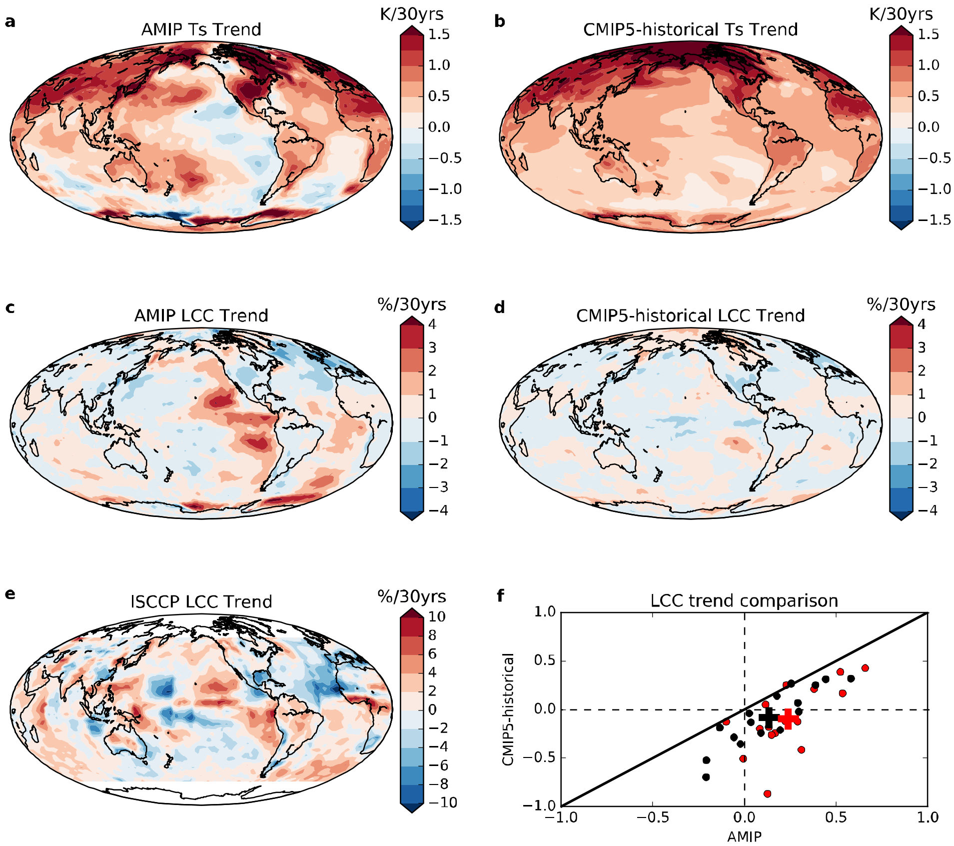

Figure 3. Comparison of recent T_s and LCC trends in AMIP (1980-2005), CMIP5-historical (1980-2005), and satellite observations (1983-2005). (a-d) Ensemble mean surface temperature and LCC trend in AMIP and historical simulations. (e) LCC trend calculated from artifact-corrected ISCCP satellite data[21,22]. Note that the color bar of (e) is different from (c-d). (f) AMIP LCC trends plotted against CMIP5-historical LCC trends, for tropical (red) and global (black) averages, respectively (%/30yrs). The solid black line is the equal-value line, and crosses denote model ensemble mean values.

Methods

To carry out the PSST experiment, we first calculate the monthly global surface skin temperature anomalies $\Delta T_s(t)$ in AMIPFF experiments. In our uniform warming experiment, 1K of uniform SST warming would increase the global surface temperature by ~1.1K in CAM5.3, so we subtract $\Delta T_s(t)/1.1$ from the historical SST for each month and each location, and use the modified SST as boundary conditions. Then ΔT_s in the PSST experiment is near zero over the whole period (Supplementary Figure 14), but the SST pattern anomalies are identical to those in the AMIP simulations.

Additional experiments are designed to calculate cloud feedback under uniform and patterned long-term global warming. First, we fix the SST and climate forcings at year 2000, and run for 16 years. Then we increase the SST by 4K uniformly and reset the initial conditions, and run for another 16 years. Then the cloud feedback under uniform warming (λ_c) was calculated as the ΔR_{cloud} difference normalized by surface temperature difference between the latter 15 years of the two simulations. λ_c is close to the cloud feedback under patterned long-term warming (Fig. 1b), which is calculated with the same method, except that the SST of year 2000 is warmed by the long-term warming pattern derived from the ensemble mean of abrupt4xCO2 simulations (Supplementary Figure 7).

Cloud-induced radiation anomalies (ΔR_{cloud}) are calculated by removing cloud masking effects from cloud radiative effect anomalies using radiative kernels[29], where cloud radiative effect is defined as the difference in upwelling radiation between clear- and all-sky scenes. LCC in CAM5.3 simulations is calculated by the model using the model's level-by-level cloud fraction field and its cloud overlap assumption. For AMIP and CMIP5-historical simulations, LCC is approximated as the maximum cloud fraction between the surface and 680 hPa, which is useful for qualitative comparisons[30,9].

To calculate decadal anomalies, we first calculate annual anomalies by removing the climatological mean from annual mean values. Then a 9-year moving average is applied to filter out interannual signals.

In Fig. 2, ΔT(up,trp) is calculated as the surface temperature difference between SST averaged over tropical strong ascent regions and SST averaged over the entire tropics at each time step. Tropical strong ascent regions are defined as those with monthly 500 hPa vertical velocity magnitude $|\omega_{500}|$ exceeding the median $|\omega_{500}|$ in regions with $\omega_{500}<0$. The coefficients of ΔEIS and ΔSST in Fig. 2(c) and of ΔT(up,trp) and ΔSST in Fig. 2(d) are derived from multiple linear regression.

Data and code availability. The CESM1.2.1-CAM5.3 source code was downloaded from the CESM official website http://www2.cesm.ucar.edu/. The CAM5.3 simulation results and code used for the analyses of this study are available from the corresponding author upon request. The CMIP5-historical/AMIP data is available from the Earth System Grid - Center for Enabling Technologies (ESG-CET) website, http://pcmdi9.llnl.gov.

References

29. Soden, B. J. *et al.* Quantifying climate feedbacks using radiative kernels. *J. Climate* **21**, 3504–3520 (2008).

30. Noda, A. T., & Satoh, M. Intermodel variances of subtropical stratocumulus environments simulated in CMIP5 models, *Geophys. Res. Lett.* **41**, 7754–7761 (2014).

Supplementary Information

for

Impact of decadal cloud variations on the Earth's energy budget

Chen Zhou*, Mark D. Zelinka, and Stephen A. Klein

Lawrence Livermore National Laboratory, Livermore, CA, USA

*zhou8@llnl.gov

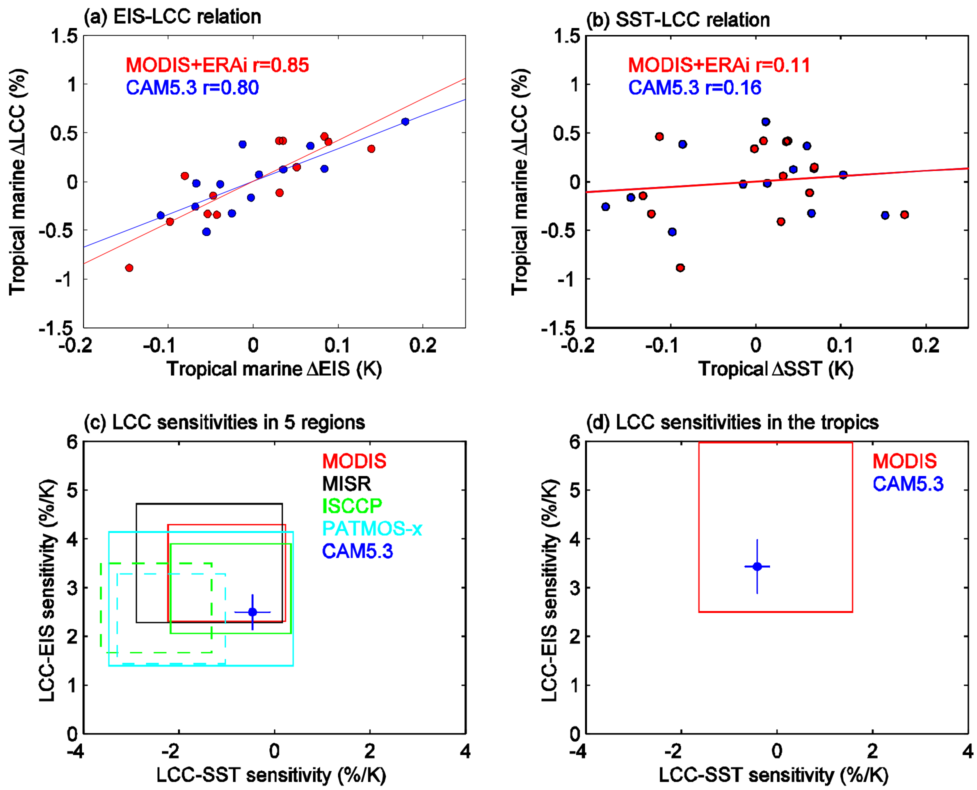

Supplementary Figure 1. Diagnosis of marine LCC sensitivity to major low cloud controling factors in CAM5.3 AMIPFF simulation. (a) Relationship between tropical mean annual anomalies in marine EIS[1] and marine LCC between March 2000 and February 2013. In both CAM5.3 AMIPFF simulation (blue) and observations (red), tropical marine EIS anomalies are positively correlated with marine LCC anomalies. Observational EIS is calculated from ERA-interim data[2] using equation (3) of Qu et al. 2014[3], and LCC is calculated from Terra MODIS level 3 data[4]. (b) Relationship between tropical mean annual anomalies in SST and marine LCC. (c) Sensitivity of LCC to EIS and SST in 5 subtropical low cloud regions defined by Qu et al. 2014[3]. The sensitivities are calculated from multiple linear regression, and the boxes denote the uncertainty intervals calculated from observations. Since the artifacts of ISCCP and PATMOS-x are large during the 1980s and 1990s[5,21], values calcuated from the full period of ISCCP and PATMOS-x are marked with dashed boxes, and the solid boxes for ISCCP and PATMOS-x are values calculated using data after 1996 and 1997, respectively. These observational values are from Qu et al. 2015[7]. (d) LCC sensitivity to EIS and SST over the whole tropical ocean, calculated from multiple linear regression of tropical marine LCC annual anomalies against marine EIS and SST annual anomalies. Based on these plots, we conclude that marine LCC sensitivities calculated from CAM5.3 are generally within the uncertainty interval of observations.

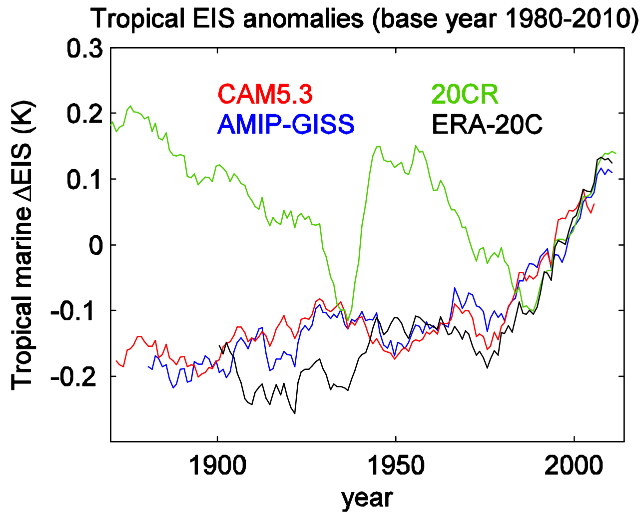

Supplementary Figure 2. Comparison of 9-year smoothed tropical marine EIS anomalies in ERA-20C reanalysis[8], 20CR reanalysis[9], AMIP-GISS simulations (the only AMIP model covering the whole 20^{th} century), and our CAM5.3 AMIP-like simulations. The base period to calculate anomalies is 1980-2010. We conclude CAM's simulation of increasing EIS trend during the satellite era (1979-present) is in agreement with that of other available models. Prior to the satellite era, EIS does not vary by more than by 0.2 K in 3 out of 4 available estimates including that of CAM5.3.

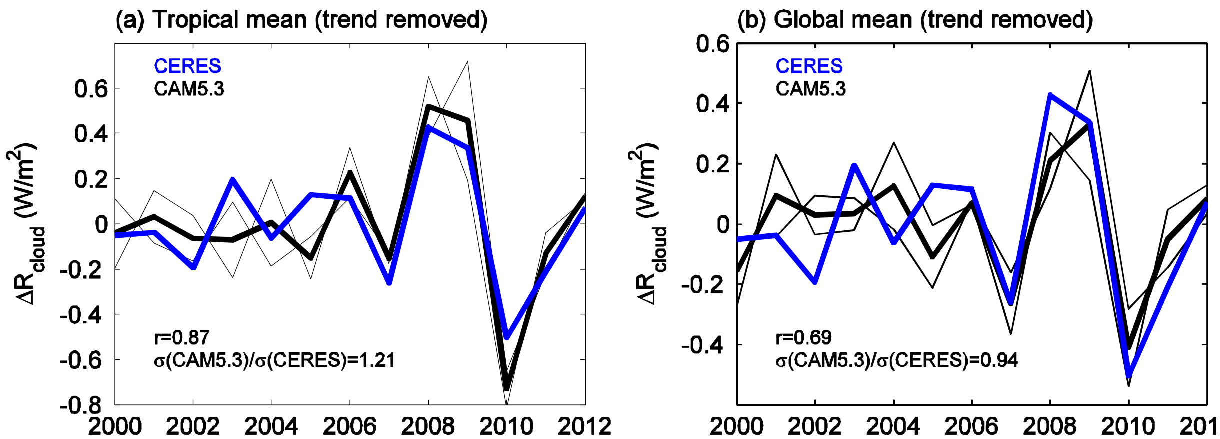

Supplementary Figure 3. Comparison of detrended ΔR_{cloud} in observations and CAM5.3 AMIPFF simulations. The cloud masking effect in CERES cloud radiative effect is removed with ERA-Interim data and radiative kernels[29] following Dessler 2013[11]. Thin black lines are calculated from individual runs, and thick black lines are calculated from ensemble mean values. Correlation coefficients between the CERES and CAM5.3 ΔR_{cloud} time series and the ratio of their standard deviations are displayed in the lower left corner of the plots. We conclude that CAM's simulation of interannual ΔR_{cloud} is in reasonable agreement with the satellite observations.

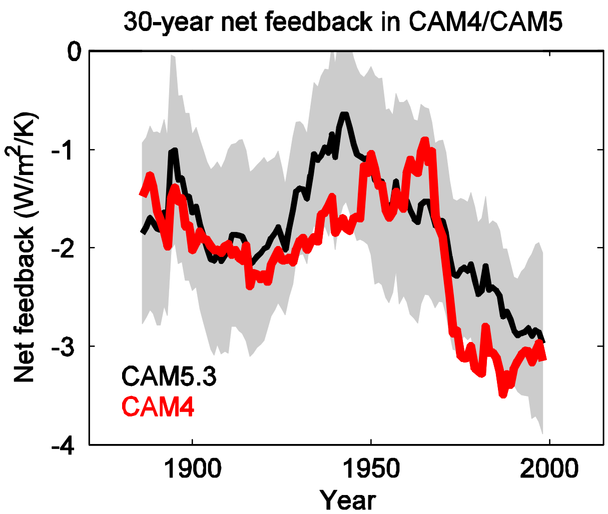

Supplementary Figure 4. Comparison of 30-year net feedback paramters in CAM4 and CAM5.3. Black solid line is calculated from the net TOA radiation and T_s anomalies averaged over the AMIPFF simulations, which is same as the black line in Fig. 1(a). Red line represents results calculated from an independent CAM4 AMIPf2000 experiment. CAM4[12] differs markedly from CAM5[13] in nearly all of its physical parameterizations and thus can be considered to be the result of a mostly independent model. Although not perfect, there is general agreement between CAM4 and CAM5.3 on the decadal variations in the net feedback, particularly for its more negative values after 1980.

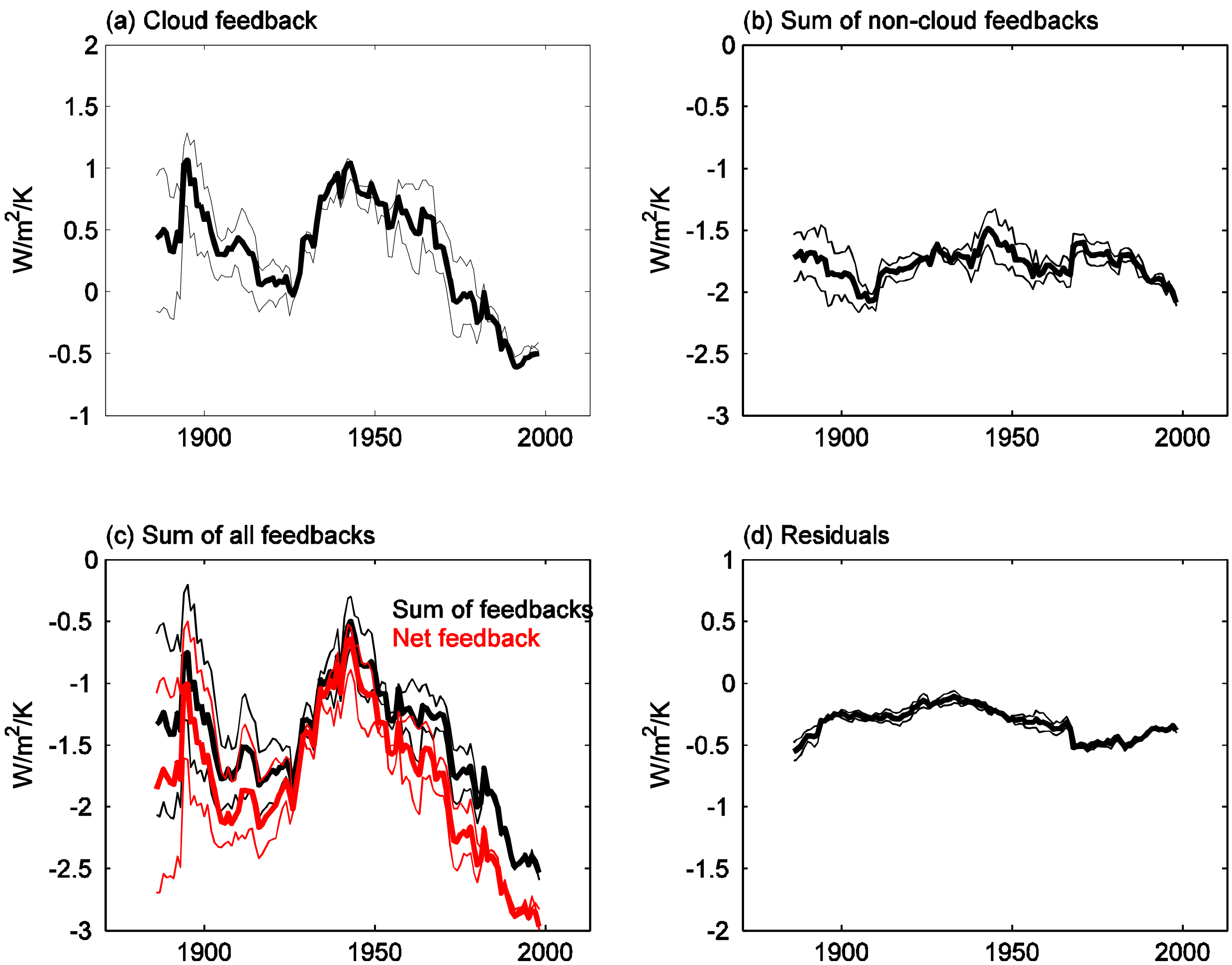

Supplementary Figure 5. Evolution of decadal cloud feedback and non-cloud feedbacks. (a) 30-year cloud feedback estimates from AMIPFF simulations. (b) Sum of Planck, lapse rate, water vapor, and surface albedo feedbacks. (c) Comparison of the sum of feedbacks calculated from kernels (black) and the net feedback calculated from TOA fluxes (red). (d) Difference between the net feedback calculated from TOA fluxes and the sum of feedbacks calculated from kernels. The residual term includes kernel errors, cross-field correlations. Clearly, the variance of cloud feedback is much larger than the non-cloud feedbacks, indicating the importance of decadal cloud feedback in driving variations in decadal net feedback.

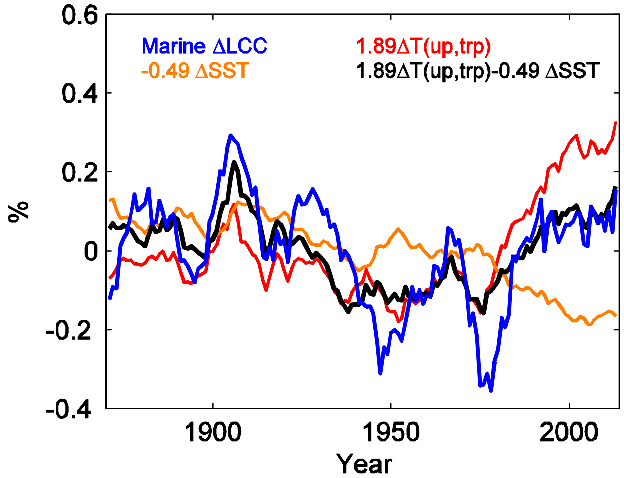

Supplementary Figure 6. Relationship between tropical marine ΔLCC (blue), ΔT(up,trp) (red) and tropical ΔSST (orange), and the linear combination of ΔT(up,trp) and ΔSST (black). All time series are ensemble mean values of 9-year moving averages from individual runs. The coefficients of ΔT(up,trp) and ΔSST (black) are calculated by substituting the regression for EIS (Fig. 2d) as a function of ΔT(up,trp) and ΔSST into the regression equation for ΔLCC (Fig. 2c). In doing so, one arrives at a relationship between ΔLCC and ΔSST and ΔT(up,trp), that allows one to explore the relative influences on low cloud cover of the mean SST and the difference in SST between tropical ascent and descent regions. ΔLCC is well correlated with the linear combination of ΔT(up,trp) and ΔSST (black) (r=0.77), moderately correlated with ΔT(up,trp) (r=0.51), and poorly correlated with ΔSST (r=-0.06). Therefore, the decadal changes in ΔLCC are controlled by both ΔT(up,trp) and ΔSST, with the former playing the more important role. Please see Supplementary Text 1 for further discussion.

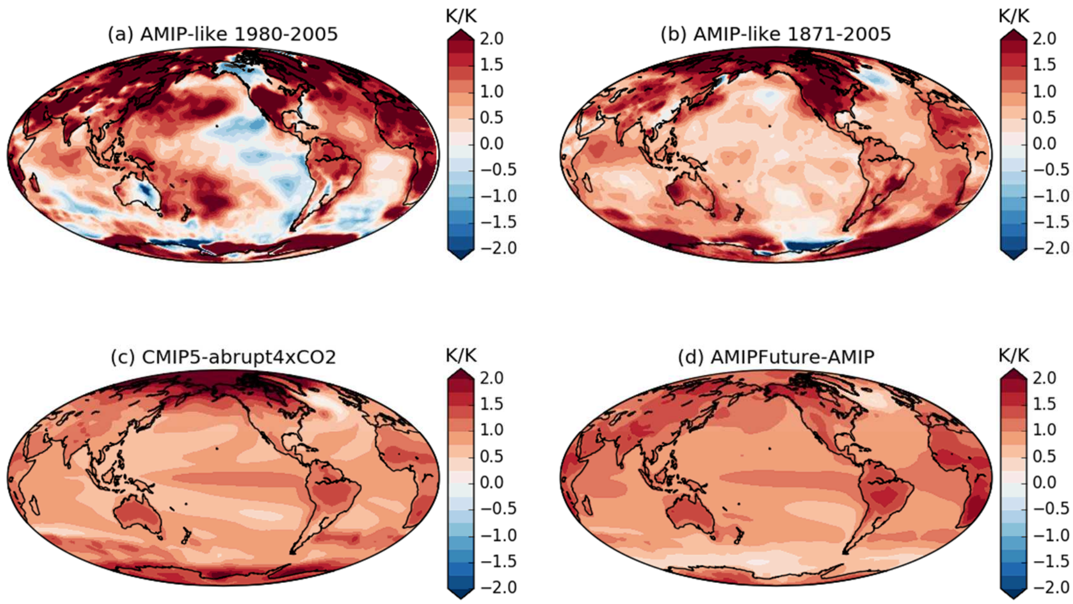

Supplementary Figure 7. Normalized surface temperature trend from the (a) AMIP-like simulation over the period 1980-2005, (b) AMIP-like simulation over the period 1871-2005, (c) ensemble mean CMIP5-abrupt4xCO_2 simulations over years 1 to 150 of the experiment, and (d) ensemble mean difference between AMIPFuture (AMIP plus a patterned future warming) and AMIP simulations. The local surface temperature anomalies are normalized by the global mean surface temperature change for better comparison, so the units are K/K. The spatial pattern of warming observed in the recent past (panel a) is significantly more spatially inhomogeneous than that expected for global warming over the next century (panels c and d).

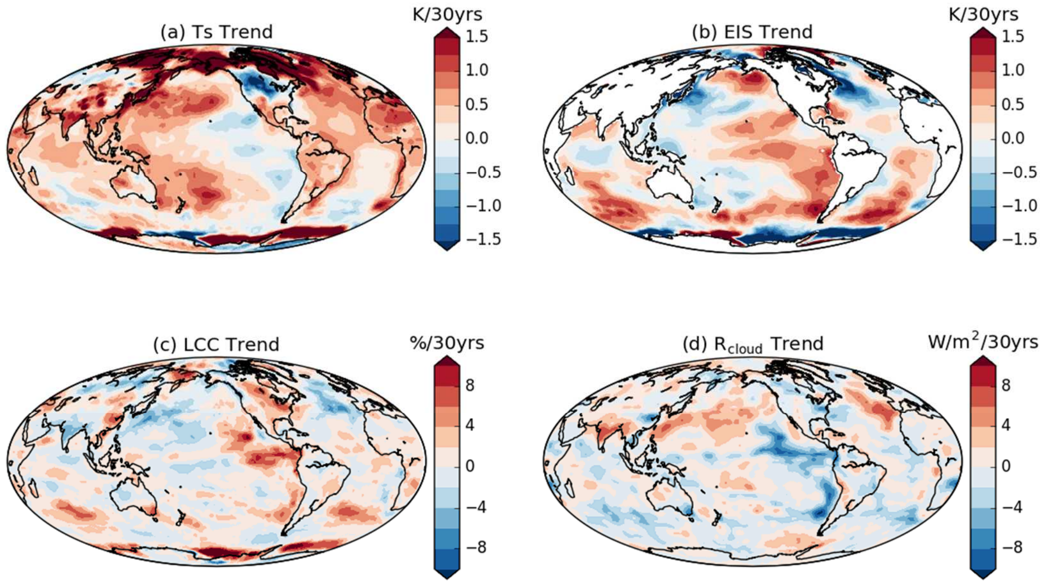

Supplementary Figure 8. Spatial correspondence among trends in cloud-controlling factors, low cloud cover, and cloud-induced radiation anomalies. Trends in (a) surface temperature, (b) EIS, (c) LCC and (d) R_{cloud} in the AMIPFF experiment between 1980 and 2005. In regions where EIS increases, LCC increases and R_{cloud} decreases, supporting our physical mechanism.

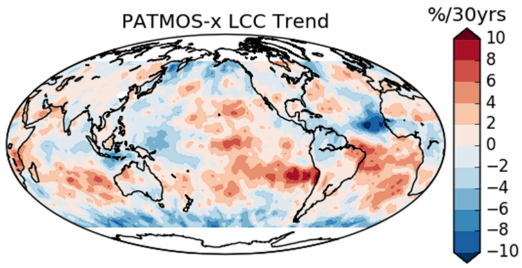

Supplementary Figure 9. LCC trend for the years 1983-2005 calculated from corrected PATMOS-x data[5,21]. Although not in perfect agreement, PATMOS-x and ISCCP (Figure 3e) data agree on the increases in LCC over the tropical Eastern Pacific, Southern Indian and Southern Atlantic oceans.

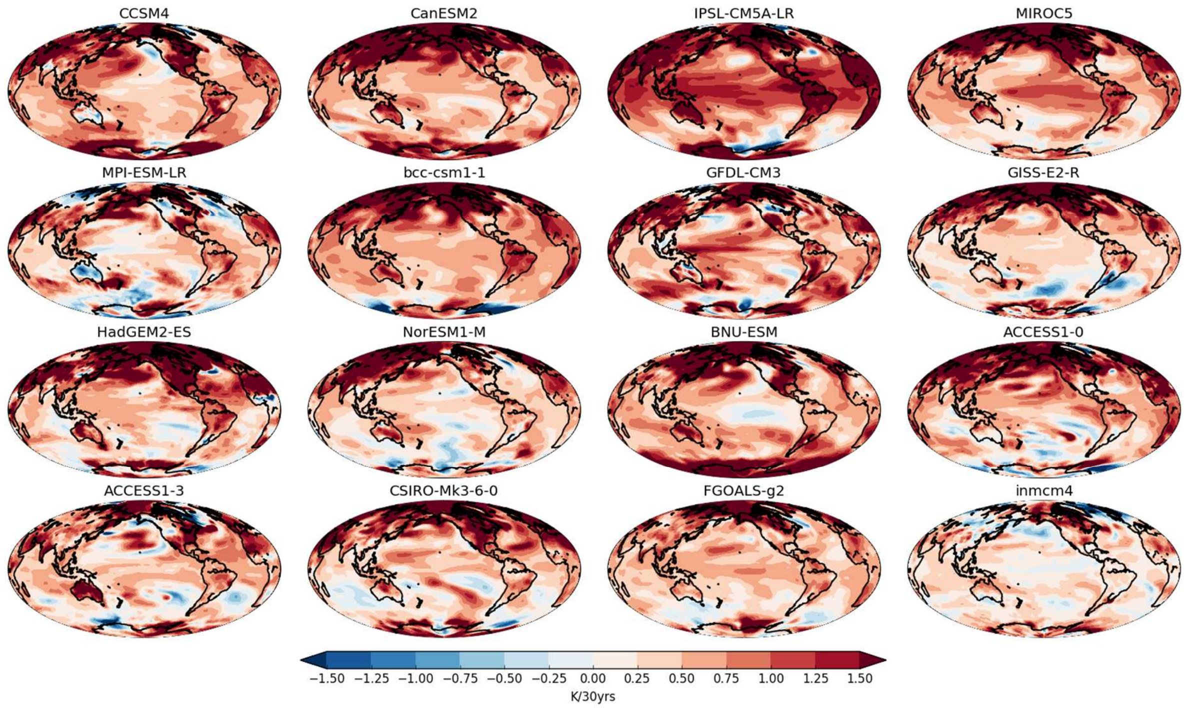

Supplementary Figure 10. Surface temperature trend in CMIP5-historical simulations during 1980-2005, divided by the global mean surface temperature trend (K/30yrs). None of these coupled models show as strong temperature decrease in the tropical Eastern Pacific Ocean as in AMIP simulations.

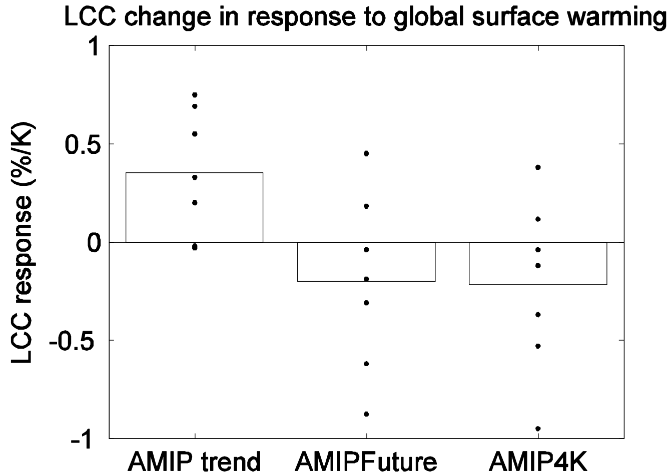

Supplementary Figure 11. Responses of global mean LCC to changes in global mean surface temperature, in AMIP, AMIP-Future and AMIP4K simulations. Left column is calculated from AMIP trend (1980-2005), middle column is calculated from the difference between AMIP-future (AMIP plus a patterned future warming) and AMIP, and right column is calculated from the difference between AMIP-4K (AMIP plus a 4K uniform warming) and AMIP. LCC is calculated from the ISCCP simulator[14,15], LCC=$C_{680\text{-}1000hPa}/(1-C_{0\text{-}680hPa})$. LCC calculated from ISCCP simulator is more accurate than the maximum value of cloud fraction between 680 and surface, but ISCCP simulator results are only available for a small subset of CMIP5-historical models, so we use the latter method in Fig. 3[16,9]. Models generally predict increased LCC in response to the warming pattern of the last 30 years in contrast to that predicted for global warming.

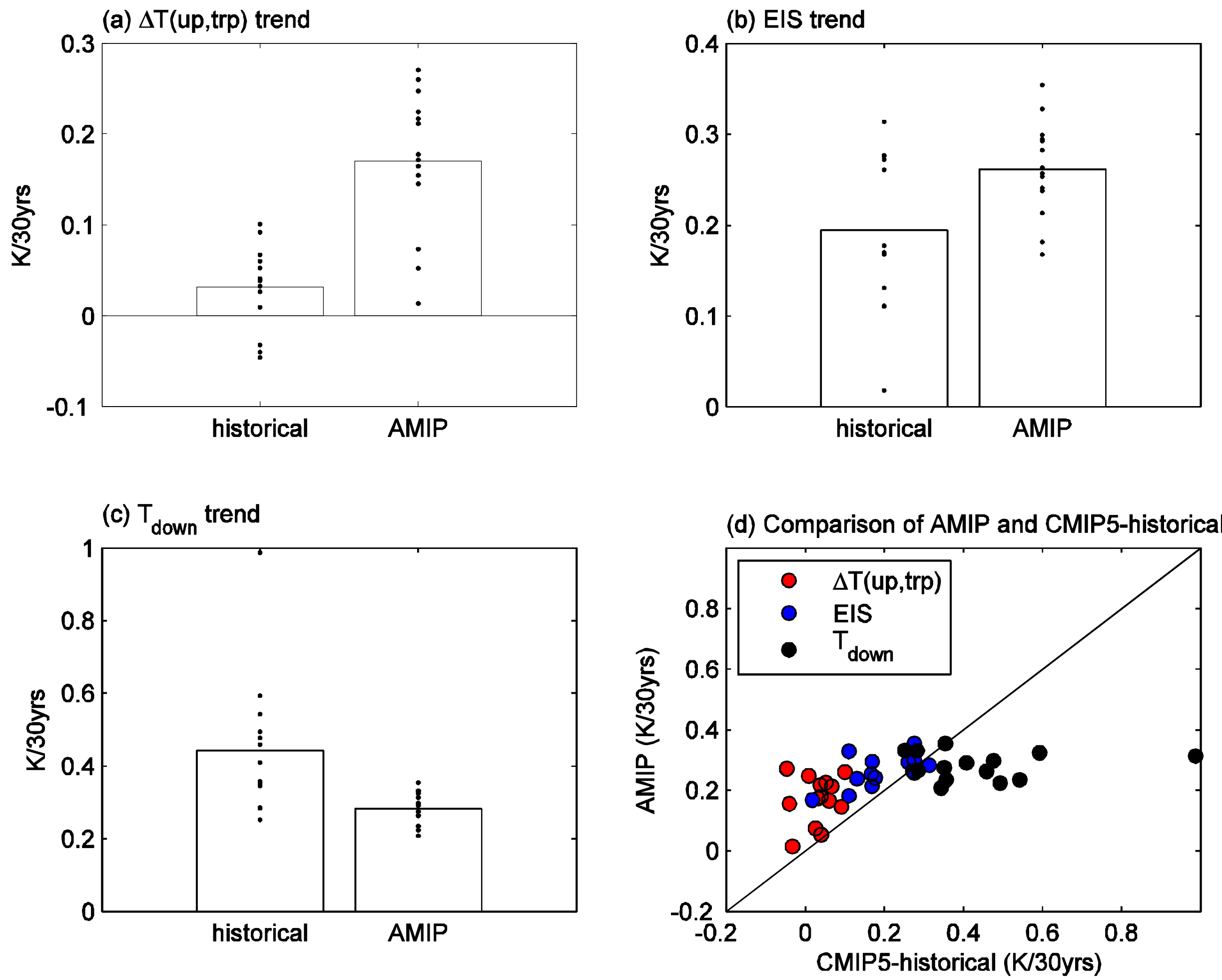

Supplementary Figure 12. Comparison of trends over the period 1980-2005 in AMIP and CMIP5-historical simulations. (a) SST difference between tropical ascent regions and the tropical mean values. (b) Tropical marine EIS trend. (c) SST trend in tropical descent regions, defined as those with monthly 500 hPa vertical velocity magnitude $|\omega_{500}|$ exceeding the median $|\omega_{500}|$ in regions with $\omega_{500}>0$. (d) Trends in (red) ΔT(up,trp), (blue) EIS, and (black) T_{down} in CMIP5-historical simulations plotted against those in AMIP simulations. EIS and ΔT(up,trp) changes in AMIP simulations are systematically larger than those in CMIP5-historical simulations, and T_{down} changes in AMIP simulations are smaller than those in CMIP5-historical simulations in most models. Therefore, the LCC trend in AMIP is systematically larger than in CMIP5-historical.

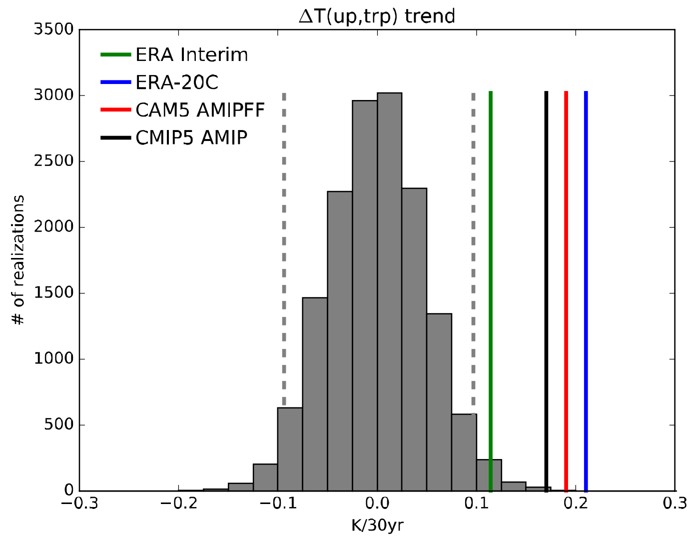

Supplementary Figure 13. Comparing modeled and observed tropical SST trends. Histogram of ΔT(up,trp) trends from all overlapping 26-year periods in piControl simulations. Dashed gray lines indicate the 2.5th and 97.5th percentiles. The 1980-2005 ΔT(up,trp) trends determined using AMIP SSTs and ω_{500} from ERA Interim (green), from ERA-20C (blue), from CAM5 AMIPFF simulations (red), and from CMIP5 AMIP simulations (black, averaged over all simulations) are within but on the extreme tail of the piControl trend distribution. Please see Supplementary Text 2 for further discussion.

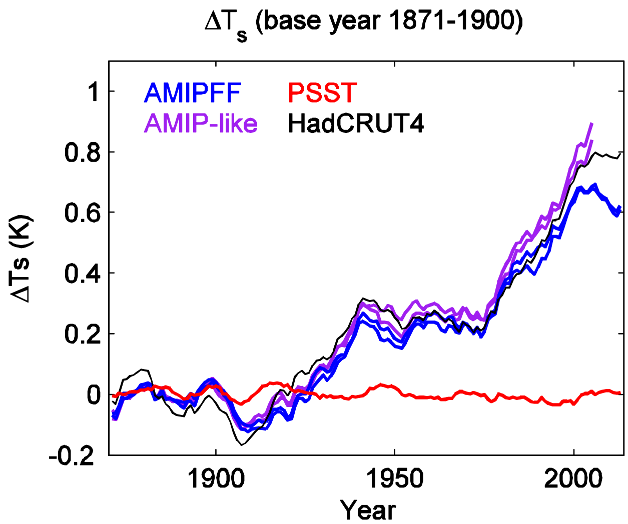

Supplementary Figure 14. 9-year smoothed global surface temperature anomalies. The surface temperature in AMIP-like and AMIPFF simulations increases significantly, but remains roughly unchanged in the PSST simulation. ΔT_s in AMIP-like is consistent with HadCRUT4 observations[18]. ΔT_s in AMIPFF simulations increases less than in AMIP-like simulations because the CO_2 concentration remains unchanged in AMIPFF simulations.

Supplementary Table 1. List of models used in AMIP and CMIP5-historical simulations

Climate Center	**CMIP5-historical**	**CMIP5-AMIP**
ACCESS	ACCESS1-0	ACCESS1-0
ACCESS	ACCESS1-3	ACCESS1-3
BCC	bcc-csm1-1	bcc-csm1-1*
GCESS/BNU	BNU-ESM	BNU-ESM
CCC	CanESM2	CanAM4*
NCAR	CCSM4	CCSM4*
CSIRO/QCCCE	CSIRO-Mk3-6-0	CSIRO-Mk3-6-0
LASG/IAP	FGOALS-g2	FGOALS-g2
GISS	GISS-E2-R	GISS-E2-R
GFDL	GFDL-CM3	GFDL-CM3
MOHC	HadGEM2-ES	HadGEM2-A*
INM	inmcm4	inmcm4
IPSL	IPSL-CM5A-LR	IPSL-CM5A-LR
MIROC	MIROC5	MIROC5
MPI	MPI-ESM-LR	MPI-ESM-LR*
NCC	NorESM1-M	NorESM1-M
MRI		MRI-CGCM3*

Note: The first ensemble member (r1i1p1) from each model is used, except that we use r7i1p1 from AMIP-CCSM4 because it is first member with *clisccp* output available.

The sign * denotes models used in Supplementary Figure 11.

Supplementary Text 1. Physical Mechanisms Driving Decadal Changes in Low Cloud Cover

Here we present in greater detail the physical mechanisms that drive the changes in tropical low cloud cover (LCC) over the 20th century.

Variations in LCC over the subsidence regions of the tropical oceans on seasonal and inter-annual time-scales have been observed to be highly sensitive to changes in the strength of the temperature inversion that caps the planetary boundary layer[19,1]. This sensitivity arises physically because a stronger temperature inversion limits the rate of mixing between the boundary layer and the free troposphere above. With less mixing, the drying and warming effects of mixing in free-tropospheric air are reduced with the consequence that the boundary layer is colder, moister, and hence more cloudy. Large-eddy simulations have confirmed the mechanisms of this observed sensitivity[20,21]. Thus, it is expected that LCC variations on decadal time-scales would also be sensitive to inversion strength[22]. The tropical inversion strength essentially measures the warmth of free tropospheric temperatures relative to that of the boundary layer; thus, it is essential to understand what controls these temperatures and their relationships to tropical SST.

To a first approximation, free tropospheric temperatures throughout the tropics are most sensitive to SST in tropical ascent (i.e., deep convective) regions. This is because the moist adiabat of the tropical free troposphere is controlled by the moist static energy of the rising air in deep convective clouds of tropical ascent regions and this moist static energy is closely related to the local SST. Thus, if SST in tropical ascent regions increases, there will be free tropospheric warming in tropical ascent regions which atmospheric dynamics will spread to free tropospheric descent regions through the "weak-temperature gradient" approximation[20]. In absence of SST changes in the tropical descent regions, the increase in free tropospheric temperatures will increase the lower tropospheric inversion strength in the tropical descent regions and hence increase LCC in tropical descent regions. On the other hand, if SST in tropical descent regions decreases without any change in SST in tropical ascent regions, the boundary layer air in tropical descent regions will cool without any changes to free tropospheric temperatures. In this situation, the inversion strength increases causing LCC to increase. And if difference between SST in the tropical ascent and descent regions remains fixed, then there would be no change in inversion strength – following directly from the definition of EIS[1]– and hence LCC would remain fixed. This is the primary physical mechanism by which LCC is so very sensitive to variations in the SST patterns, or more specifically the difference in SST between tropical ascent and descent regions.

While this is the primary mechanism at work relating variations in the SST pattern with the tropical inversion strength and LCC, we account for two additional secondary effects that happen when the mean SST in the tropics changes but the SST difference between the tropical ascent and descent regions remains fixed. First, as shown by LES studies[20,21] and supported by observational analyses[3,7,24], LCC decreases when SST increases and EIS remains fixed.

Physically, this is usually explained as more efficient drying of the boundary layer as the temperature rises by circulations at either turbulent[18] or larger[16] scales. This is why our study – following past studies[3,7,24] – predicts LCC variations with a multi-linear model involving two parameters, EIS and SST (Fig. 2c). We note that CAM is consistent with the observed sensitivities of LCC to EIS and SST (Supplementary Figure 1). Second, for reasons that are not yet clear, climate models simulate free tropospheric warming that is slightly greater than that predicted from moist adiabatic warming in tropical ascent regions. (Note that "moist adiabatic warming" here is defined as that resulting from an increase in surface air moist static energy that comes purely from an air temperature increase identical to that of the underlying SST with no change in relative humidity.) This enhanced free tropospheric warming was shown to be a robust, but unexplained feature, of climate models by Qu et al.[27] in their analysis of aqua-planet experiments with uniform warming. This is why we include the mean SST as an additional predictor in the explanation of EIS variations (Fig. 2d). We find that EIS increases with the mean SST, like that found in the models analyzed by Qu et al.[27]. Inclusion of these secondary effects does not change the dominance of the SST difference between tropical ascent and descent regions in driving decadal variations in EIS and LCC, although the inclusion of a dependency on the mean temperature induces a general decrease in LCC and a slight increase in EIS over the 20th century (Supplementary Figure 6 and Fig. 2d).

Thus, these secondary effects, while helpful in quantitatively explaining the century time-scale variations in EIS and LCC, do not alter the main explanation. To repeat the main explanation, fluctuations in the pattern of warming – or more specifically the difference in warming between tropical ascent and descent regions – causes fluctuations in inversion strength and LCC and hence the radiation budget, which leads to fluctuations in the decadal cloud (and total) feedback. Because the recent warming pattern is distinctly non-uniform, with greater warming in tropical ascent regions and relative cooling in tropical descent regions, the decadal cloud feedback over the period 1980-2005 is negative and deviates strongly from the positive feedback under long-term warming pattern.

Supplementary Text 2. Assessing the Ability of Coupled Climate Models to Simulate the SST Trends Observed over 1980-2005

An important question is whether the systematic differences shown in Figure 3f arise because coupled models are incapable of simulating a warming pattern like that observed between 1980-2005 or because they can, but just didn't happen to do it in years 1980-2005 of the historical runs.

The observed SST trend pattern over the 26-year period 1980-2005 is an unknown combination of forced and unforced changes. Our null hypothesis is that the trend pattern is dominated by internal variability. An alternative hypothesis is that the SST trend pattern is primarily forced and that coupled climate models cannot reproduce it because of model deficiencies and/or incorrect imposed forcing.

While it is not possible to rule out forcing as contributing to the observed pattern, we can determine whether unforced coupled models are capable of simulating the observed pattern. To do so, we compute all possible 26-year SST trends in fully coupled piControl runs of CMIP5 models. If we could find trends that match those observed between 1980 and 2005, we could conclude that (1) models are capable of reproducing the observed SST trends but they just happened to not do so during the AMIP period and (2) that the trend can emerge solely due to internal variability and does not require forcing.

Because it is the primary driver of tropical mean EIS anomalies and hence LCC anomalies (Fig. 2d), we compare modeled and observed trends in $\Delta T(up,trp)$ – the difference between the SST in tropical ascent regions and the tropical mean SST. In Supplementary Figure 13, we show the histogram of $\Delta T(up,trp)$ trends from all overlapping 26-year periods in all available piControl simulations with the necessary output. The 1980-2005 $\Delta T(up,trp)$ trends determined using AMIP SSTs and ω_{500} from ERA Interim (green), ERA-20C (blue),from CAM5 AMIPFF simulations (red), and from CMIP5 AMIP simulations (black, averaged over all simulations) are within but clearly on the tail of the distribution, exceeding the 97.5th percentile of all possible piControl trends. Specifically, out of 15,186 total piControl $\Delta T(up,trp)$ trends, only 1 exceeds the AMIP trend derived using ω_{500} from ERA-20C or CAM5 AMIPFF, 8 exceed the AMIP trend derived using ω_{500} from CMIP5 AMIP, and 214 exceed the AMIP trend derived using ω_{500} from ERA-Interim. These results suggest that an increase in SST gradient between ascent regions and the rest of the tropics that is as large as observed over 1980-2005 occurs very rarely (1% of the time or less) in unforced simulations.

If the models accurately capture or overestimate unforced internal variability, then we conclude that the observed trend pattern is largely incompatible with pure internal variability. In this case, the observed pattern must be partly forced, and the systematic model-observation differences in Figure 3f occur because of the models systematically having an incorrect forcing or SST response to forcing. Even if the models had correct forcing and SST response to forcing, internally-generated trends in coupled historical simulations could still occur asynchronously with those in nature and lead to these systematic differences, but lack of synchronization alone cannot account for the systematic differences.

If, however, the models collectively underestimate internal variability, then the possibility remains that the observed SST trend is purely due to internal variability but that models are incapable of simulating it. In this case, the systematic differences in Figure 3f occur because of (a) the models systematically having an incorrect forcing or SST response to forcing, or (b) internally-generated trends in coupled historical simulations being of insufficient magnitude compared with those in nature, or (c) some combination of (a) and (b).

In summary, unforced coupled models are largely incapable of reproducing the spatial pattern of the observed SST trend during 1980-2005. Based on this analysis, we conclude that the systematic differences in Figure 3f cannot be explained purely by lack of synchronization between internally-generated trends in coupled historical simulations and those occurring in nature. This implies that the 1980-2005 SST trend pattern is partly forced, with systematic model-observation differences due to (a) errors the in prescribed external forcing in CMIP5-historical simulations, and/or (b) errors in the models' responses to historical forcings. Highly uncertain aerosol forcing, which has been shown to partially contribute to the SST trend pattern during recent decades[28,24], may play a role in model-observation SST trend differences. If, however, models collectively underestimate internal variability on this timescale, the possibility remains that the pattern was an unusual natural fluctuation and that models are incapable of simulating it.

Finally, we note that our paper's conclusion regarding climate sensitivity does not depend on whether the recent SST trend pattern is primarily induced by natural variability or by regional climate forcings: Long-term feedback and climate sensitivity are defined with respect to CO_2-induced global warming (which is relatively spatially uniform according to climate models and the observed SST trend during 1871-2013), so feedbacks and climate sensitivity calculated from the recent period would still likely be biased despite being forced. Indeed, an alternative to "forcing efficacies" for explaining the apparent dependence of warming on forcing agent could be that different forcings actuate feedbacks of different strength because they induce different surface temperature anomaly patterns.

References for supplementary

1. Wood, R., Bretherton C. S. On the relationship between stratiform low cloud cover and lower-tropospheric stability. *J. Clim.* **19**, 6425–6432 (2006).
2. Dee, D. P. et al. The ERA-Interim reanalysis: configuration and performance of the data assimilation system. *Quarterly Journal of the Royal Meteorological Society* **137**, 553-597 (2011).
3. Qu, X., Hall, A., Klein, S. A., & Caldwell, P. M. On the spread of changes in marine low cloud cover in climate model simulations of the 21st century. *Clim Dyn* **42**, 2603–2626 (2014).
4. Platnick, S. *et al.* The MODIS cloud products: Algorithms and examples from Terra. IEEE Trans. *Geosci. Remote Sens.* **41**, 459–473 (2003).
5. Norris, J. R. & Evan, A. T. Empirical Removal of Artifacts from the ISCCP and PATMOS-x Satellite Cloud Records. *Journal of Atmospheric and Oceanic Technology* **32**, 691-702 (2015).
6. Seethala, C., Norris, J. R., & Myers, T. A. How Has Subtropical Stratocumulus and Associated Meteorology Changed since the 1980s? *J. Climate* **28**, 8396-8410 (2015).

7. Qu, X., Hall, A., Klein, S. A. & DeAngelis, A. M. Positive tropical marine low-cloud cover feedback inferred from cloud-controlling factors. *Geophysical Research Letters* **42**, 7767-7775 (2015).
8. http://www.ecmwf.int/en/research/climate-reanalysis/era-20c/
9. Compo, G.P. *et al.* The Twentieth Century Reanalysis Project. *Quarterly J. Roy. Meteorol. Soc.* **137**, 1-28 (2011).
10. Soden, B. J. *et al.* Quantifying climate feedbacks using radiative kernels. *J. Clim.* **21**, 3504–3520 (2008).
11. Dessler, A. E. Observations of Climate Feedbacks over 2000-10 and Comparisons to Climate Models. Journal of Climate **26**, 333-342 (2013).
12. Neale, R. B. *et al.* The Mean Climate of the Community Atmosphere Model (CAM4) in Forced SST and Fully Coupled Experiments. *J. Clim.* **26**, 5150-5168 (2013).
13. Neale, R. B. *et al.* (2010), *Description of the NCAR Community Atmosphere Model (CAM 5.0), NCAR Tech. Note NCAR/TN-486+STR*, 282 pp., (Natl. Cent. for Atmos. Res., Boulder, Colo., 2010).
14. Klein, S. A. & Jakob, C. Validation and sensitivities of frontal clouds simulated by the ECMWF model. *Monthly Weather Review* **127**, 2514-2531 (1999).
15. Webb, M., Senior, C., Bony, S. & Morcrette, J. J. Combining ERBE and ISCCP data to assess clouds in the Hadley Centre, ECMWF and LMD atmospheric climate models. *Climate Dynamics* **17**, 905-922 (2001).
16. Noda, A. T., & Satoh, M. Intermodel variances of subtropical stratocumulus environments simulated in CMIP5 models, *Geophys. Res. Lett.* **41**, 7754–7761 (2014).
17. Zhou, C., Zelinka, M. D., Dessler, A. E. & Klein, S. A. The relationship between interannual and long-term cloud feedbacks. *Geophys. Res. Lett.* **42**, 10463–10469 (2015).
18. Morice, C. P., Kennedy, J. J., Rayner, N. A., & Jones, P. D. Quantifying uncertainties in global and regional temperature change using an ensemble of observational estimates: The HadCRUT4 data set. *J. Geophys. Res.* **117**, D08101 (2012).
19. Klein, S. A. & Hartmann D. L. The seasonal cycle of low stratiform clouds. *J. Clim.* **6**, 1587-1606 (1993).
20. Bretherton, C. S., Blossey, P. N. & Jones, C. R. Mechanisms of marine low cloud sensitivity to idealized climate perturbations: A single-LES exploration extending the CGILS cases. *J. Adv. Model. Earth Syst.* **5**, 1942-2466 (2013).
21. van der Dussen, J. J., de Roode, S. R., Gesso, S. Dal & Siebesma, A. P. An LES model study of the influence of the free tropospheric thermodynamic conditions on the stratocumulus response to a climate perturbation. *J. Adv. Model. Earth Syst.* **7**, 1942-2466 (2015).
22. Clement, A. C., Burgman, R. & Norris, J. R. Observational and Model Evidence for Positive Low-Level Cloud Feedback. *Science* **325**, 460-464 (2009).

23. Sobel, A. H., Nilsson, J. & Polvani, L. M., The Weak Temperature Gradient Approximation and Balanced Tropical Moisture Waves. *Journal of Atmospheric Sciences* **58**, 3650-3665 (2001).
24. Myers, T. A. & Norris, J. R. Reducing the uncertainty in subtropical cloud feedback. *Geophys. Res. Lett.* **43**, 2144–2148 (2016).
25. Bretherton, C. S. & Blossey, P. N. Low cloud reduction in a greenhouse-warmed climate: Results from Lagrangian LES of a subtropical marine cloudiness transition. *J. Adv. Model. Earth Syst.* **6**, 91–114 (2014).
26. Sherwood, S. C., Bony, S. & Dufresne, J.-L. Spread in model climate sensitivity traced to atmospheric convective mixing. *Nature* **505**, 37-42 (2014).
27. Qu, X., Hall, A., Klein, S. A. & Caldwell P. M., The strength of the tropical inversion and its response to climate change in 18 CMIP5 models. *Clim Dyn* **45**, 375-396 (2015).
28. Watanabe, M. *et al.* Contribution of natural decadal variability to global warming acceleration and hiatus. *Nature Climate Change* **4**, 893-897 (2014).
29. Takahashi C. & Watanabe M. Pacific trade winds accelerated by aerosol forcing over the past two decades. *Nature Climate Change* **6**, 768-772 (2016).